We are IntechOpen, the world's leading publisher of Open Access books Built by scientists, for scientists

6,900
Open access books available

185,000
International authors and editors

200M
Downloads

Our authors are among the

154
Countries delivered to

TOP 1%
most cited scientists

12.2%
Contributors from top 500 universities



WEB OF SCIENCE™

Selection of our books indexed in the Book Citation Index in Web of Science™ Core Collection (BKCI)

Interested in publishing with us?
Contact book.department@intechopen.com

Numbers displayed above are based on latest data collected.
For more information visit www.intechopen.com



Chapter

CFD Simulation of Flow Phenomena in Selected Centrifugal Pumps, Industrial Fans and Positive Displacement Pumps

Wieslaw Fiebig, Paulina Szwemin and Maciej Zawislak

Abstract

The chapter presents simulation models for the analysis of centrifugal pumps, fans and positive displacement pumps. In centrifugal pumps based on the "sliding mesh" method, a CFD model was created to calculate the flow characteristics, and the pump operating parameters were determined at which an unfavourable phenomenon of cavitation occurs. In the case of a radial fan, the CFD model was used to determine the influence of inlet channel geometry on the efficiency of an industrial installation. The main purpose of the CFD simulation was to obtain the pressure distributions and determine the areas in which cavitation may occur. To investigate the flow phenomena that occur in external gear pumps and double-acting vane pumps, the "immersed solid" method was used. The results of 2D and 3D simulation studies for various operating parameters of pumps have been presented.

Keywords: CFD simulation, pumps, cavitation, industrial fans, flow analysis

1. Introduction

Industrial machines and devices with rotating operating parts are difficult to model due to their complex geometry, the transition of elements of the discrete model between the rotating and non-rotating parts, the importance of the quality of elements of the discrete model, and the fact that in most cases, it is necessary to take into account the time step (elements rotate in relation to the casing). It is also troublesome that very often the calculations are stabilised only after a few rotations of the operating element. However, the use of computational fluid dynamics methods to model this group of machines and equipment is justified, as it enables:

- Determining the internal and external characteristics of machines and devices in virtual space

- Imaging and observing the flow phenomena in the machine itself (especially when for various reasons it is impossible to measure physical quantities of the flowing medium)

- Designing equipment for which there are no design guidelines (e.g. differentials, mixers)

- Improving the efficiency of machinery and equipment

In this chapter, selected examples of numerical calculations will be described, showing the possibility of using CFD methods to solve machine and equipment problems with a rotating operating element, often found in industrial practice.

2. Vane pump: flow analysis

The innovative vane pump described in study [1] was subjected to the analysis of flow phenomena. In this solution, the pump is integrated into the BLDC permanent magnet electric motor. Due to its design, which differs from the standard solutions, it was necessary to check whether cavitation could occur in the suction channel of the pump. The main objective of the CFD simulation was to determine the areas where cavitation is likely to occur [2] and its intensity depending on the rotational velocity. The subject of the study is a positive displacement pump with integrated electric drive, consisting of an impeller embedded in a casing. Unlike conventional gear and vane pumps [3–10], the pump impeller and motor stator are immovable components, while the pump casing rotates with the rotor of the electric motor. **Figure 1** shows the 3D model of the analysed pump.

An important problem is to examine the flow in the suction channel of the pump, as it is exposed to the adverse effects of cavitation, which can develop as a result of a too high value of negative pressure occurring in the suction area.

On the basis of the three-dimensional model of the pump, a geometric model of the volume of operating fluid filling its interior was prepared (**Figure 1b**). As expected, the result is a very complex structure in terms of geometry. Due to the particular interest in the phenomena occurring in the suction channel of the pump, the calculations used a fragment of the geometric model of the operating fluid volume filling the interior of the pump, which is the volume of oil filling the pump from the inlet to the suction kidneys supplying the fluid to the inter-vane spaces (**Figure 2a**). The separated volume is contained in the immovable elements of the structure, which further simplifies the formulation of the flow problem and the choice of calculation parameters.

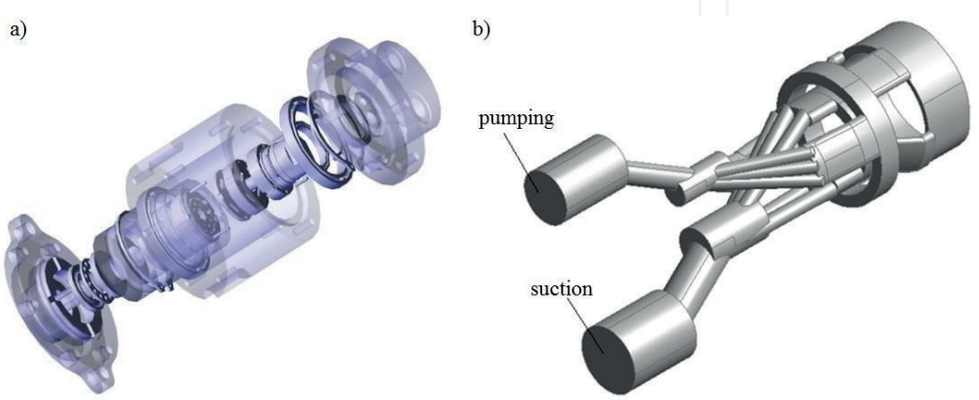


Figure 1.
(a) 3D model of the vane pump with integrated mechatronic electric drive and (b) 3D model of the operating fluid volume filling the pump.

Based on the three-dimensional pump model, the simplified geometric model of the operating fluid volume filling the suction channel was discretized using a tetrahedral grid. The result is a geometric model divided into 144,390 tetrahedral elements with 29,711 nodes, as shown in **Figure 2b**.

The next step in formulating the flow problem is to select the type and define the boundary conditions for relevant fragments of the geometry. In the analysed case, the conditions concerning the fluid inflow and outflow were set as shown in **Figure 2a**.

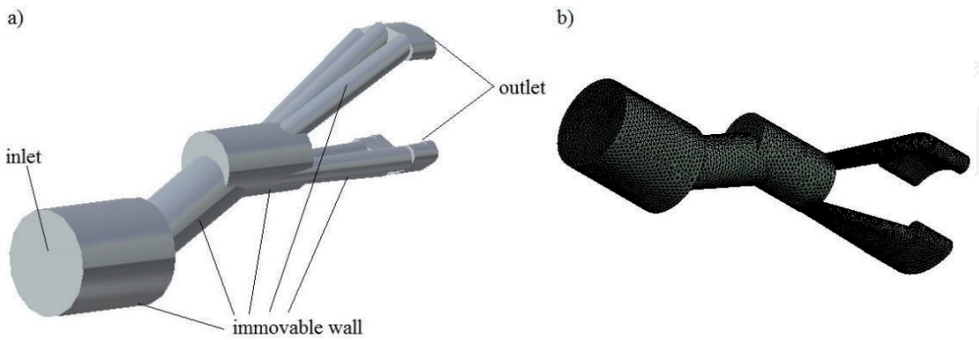


Figure 2.
(a) Suction channel geometry and (b) discrete model.

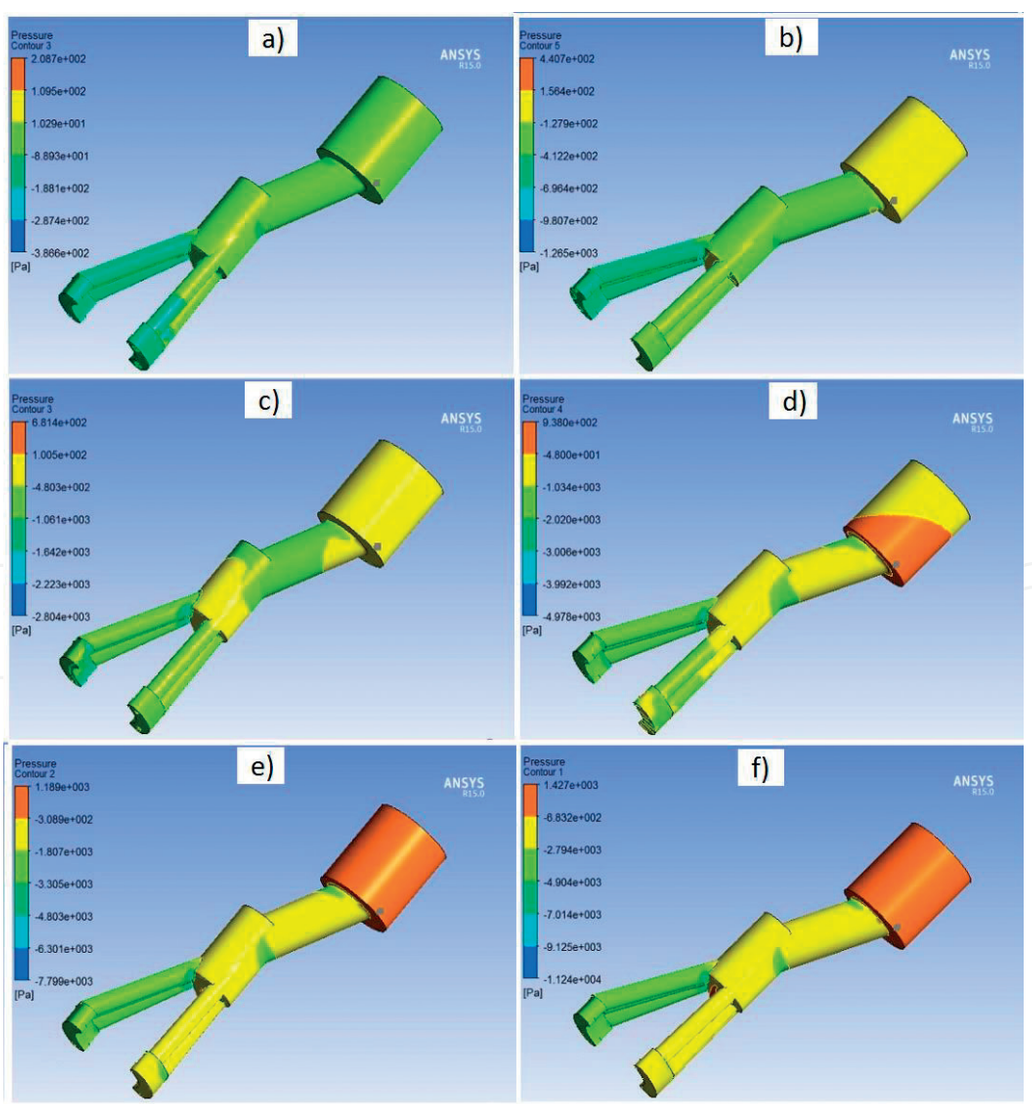


Figure 3.
Generic geometry—suction channel pressure distribution for different rotational velocities: (a) 500 rpm, (b) 1000 rpm, (c) 1500 rpm, (d) 2000 rpm, (e) 2500 rpm and (f) 3000 rpm.

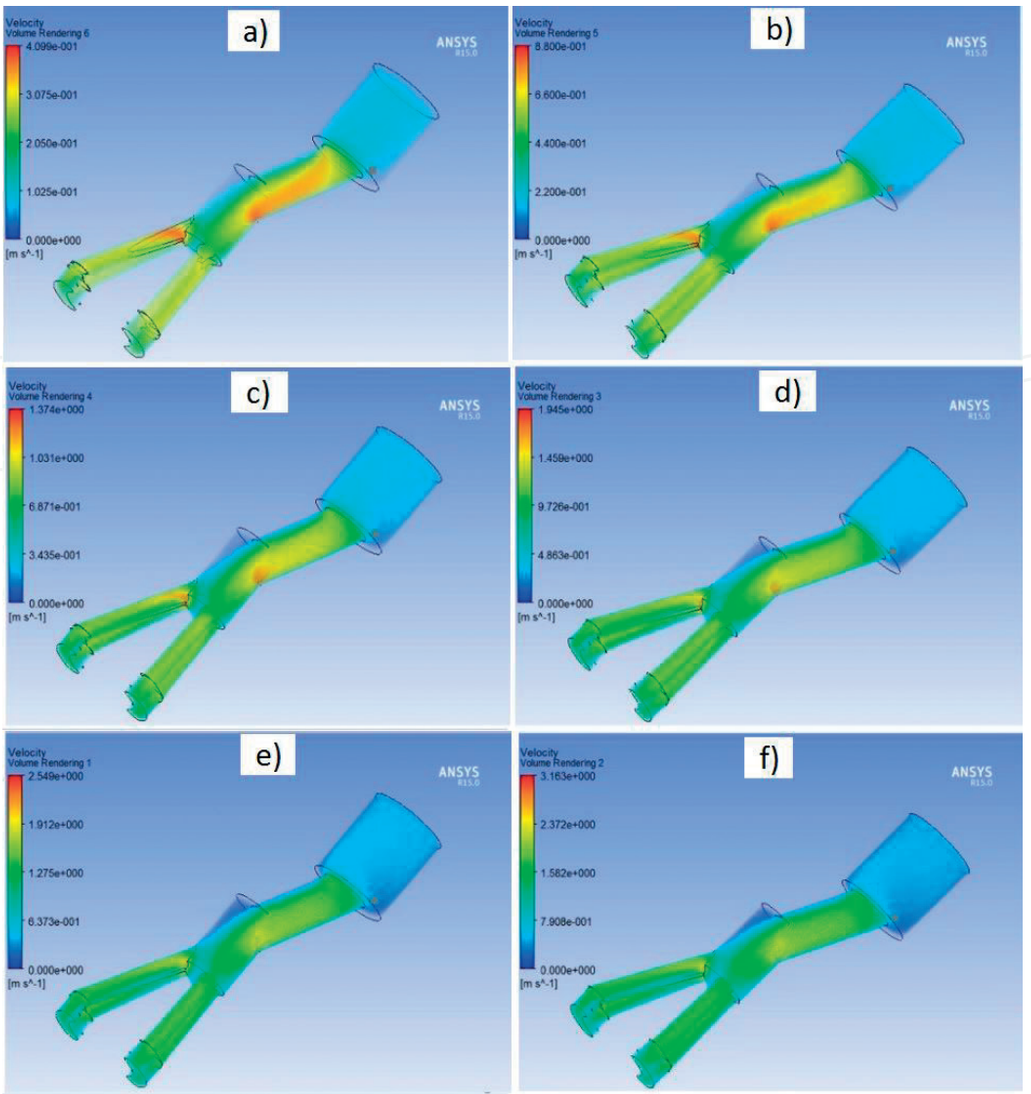


Figure 4.
Generic geometry—suction channel velocity distribution for different velocities: (a) 500 rpm, (b) 1000 rpm, (c) 1500 rpm, (d) 2000 rpm, (e) 2500 rpm and (f) 3000 rpm.

In order to obtain the most accurate results of the simulation, the "pressure inlet" condition at the inlet and the "mass flow rate" at the outlet were assumed. The mass flow rate was determined using the formula:

$$q = 2zb\left[\frac{\pi}{z}\left(R_2^2 - R_1^2\right) - w(R_2 - R_1)\right] \quad (1)$$

where q is the specific mass flow rate; z is the number of vanes; b is the width of a vane; w is the thickness of a vane; *R1* is the small race radius; and R2 is the large race radius.

On this basis, the numerical values entered into the simulation for each impeller velocity were obtained. Within the framework of the study, the analysis of the operating medium flow through the suction channel of the vane pump was performed for various rotational velocity values—changed within the range of 500–3000 rpm.

Figure 3 shows the pressure distributions in the suction channel of the tested pump for the generic geometry. For each of the cases considered, the lowest pressure occurs in one of the channels supplying fluid to the suction kidneys directly at the inlet to the channel. It was found that the negative pressures for the whole range of rotational velocities are higher than the pressure of oil evaporation, which prevents the occurrence of cavitation phenomena.

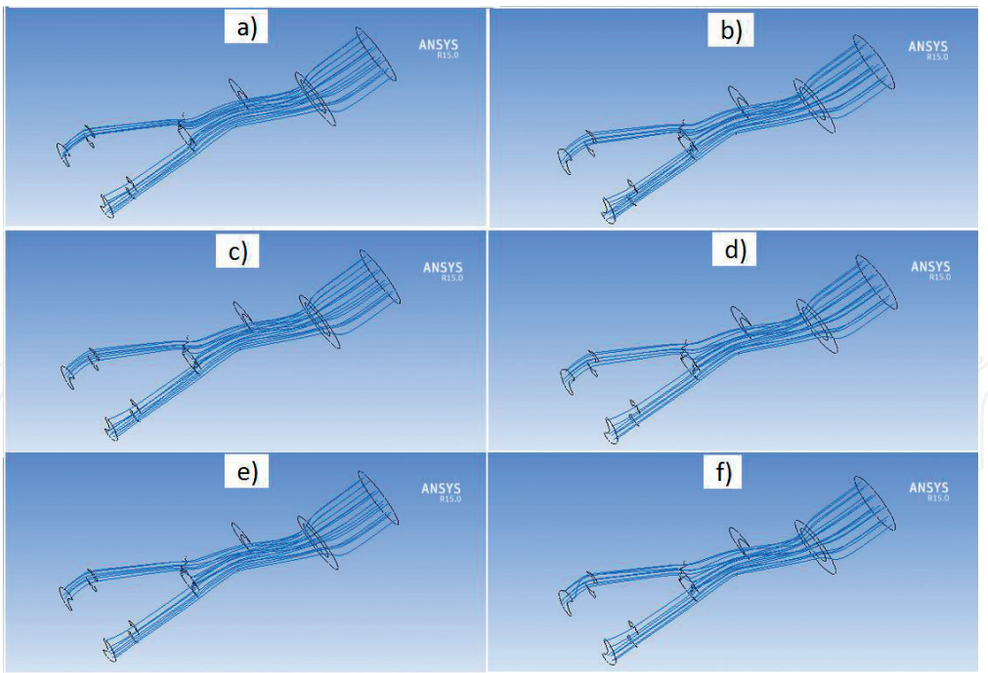


Figure 5.
Generic geometry—streamlines in the investigated suction channel area for different velocities: (a) 500 rpm, (b) 1000 rpm, (c) 1500 rpm, (d) 2000 rpm, (e) 2500 rpm and (f) 3000 rpm.

The results of the calculations, apart from pressure distributions, were presented in the form of velocity distributions in the considered area, which are presented in **Figure 4**. From the obtained velocity distributions, it appears that the rotational velocity of the pump significantly influences the velocity of fluid flow in one of the supply channels for both the generic and the modified geometry. It is worth noting that the area where the highest velocities were identified corresponds to the area of the lowest pressures observed in the suction channel. The velocity of the fluid decreases with the lowering of the rotational velocity, but in the case of simplified geometry, it is slightly lower.

Figure 5 shows the fluid flow in the form of streamlines, for which the inflow plane to the domain is assigned as the beginning. The results obtained confirm the previous assumptions that the fluid flows evenly and without major turbulences through both inlet channels. Uneven velocity distribution and different pressure values due to asymmetrical layout of channels did not affect the fluid flow. The results obtained on the basis of numerical calculations are the basis for evaluation of the structure of channels supplying fluid to the inter-vane volumes.

3. Radial fan: characteristics and performance improvement

Another object under consideration with rotating operating elements was a radial fan. The aim of the numerical simulation was to improve its efficiency. The flow of real gas through a fan with a finite amount of blades is carried out by the cost of loss of energy, called hydraulic losses. Those losses are a consequence of the friction of air molecules occurring on the blade walls and fan housing, vortexes developed in the gas stream, etc. The influence of hydraulic losses on the working characteristic of the radial fan is described by a hydraulic efficiency coefficient, which is defined as the ratio of the useful power to the power delivered by the impeller. This coefficient also defines the real delivery height to the theoretical delivery height—obtained for the finite amount of impeller blades. The impeller geometry considered in possible options, i.e. with eight (factory option) and nine (suggested option) vanes, are shown in **Figures 6** and **7**.

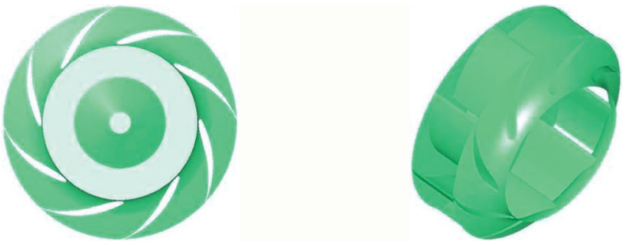


Figure 6.
Impeller shape: eight vanes.



Figure 7.
Impeller shape: nine vanes.

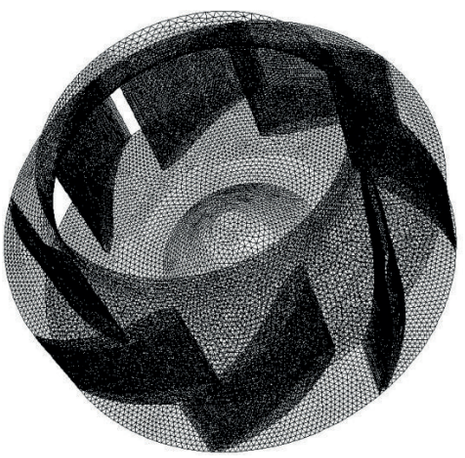


Figure 8.
Discrete model with division into tetrahedral elements on the impeller and vanes.

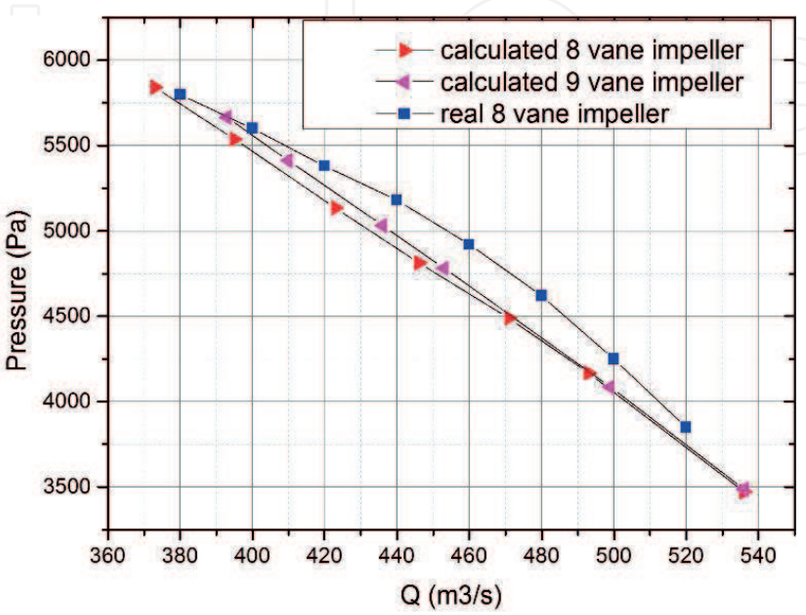


Figure 9.
Comparison of the calculation results and the results of the technical documentation for the impeller with the eight and nine vanes.

DOI: http://dx.doi.org/10.5772/intechopen.82266

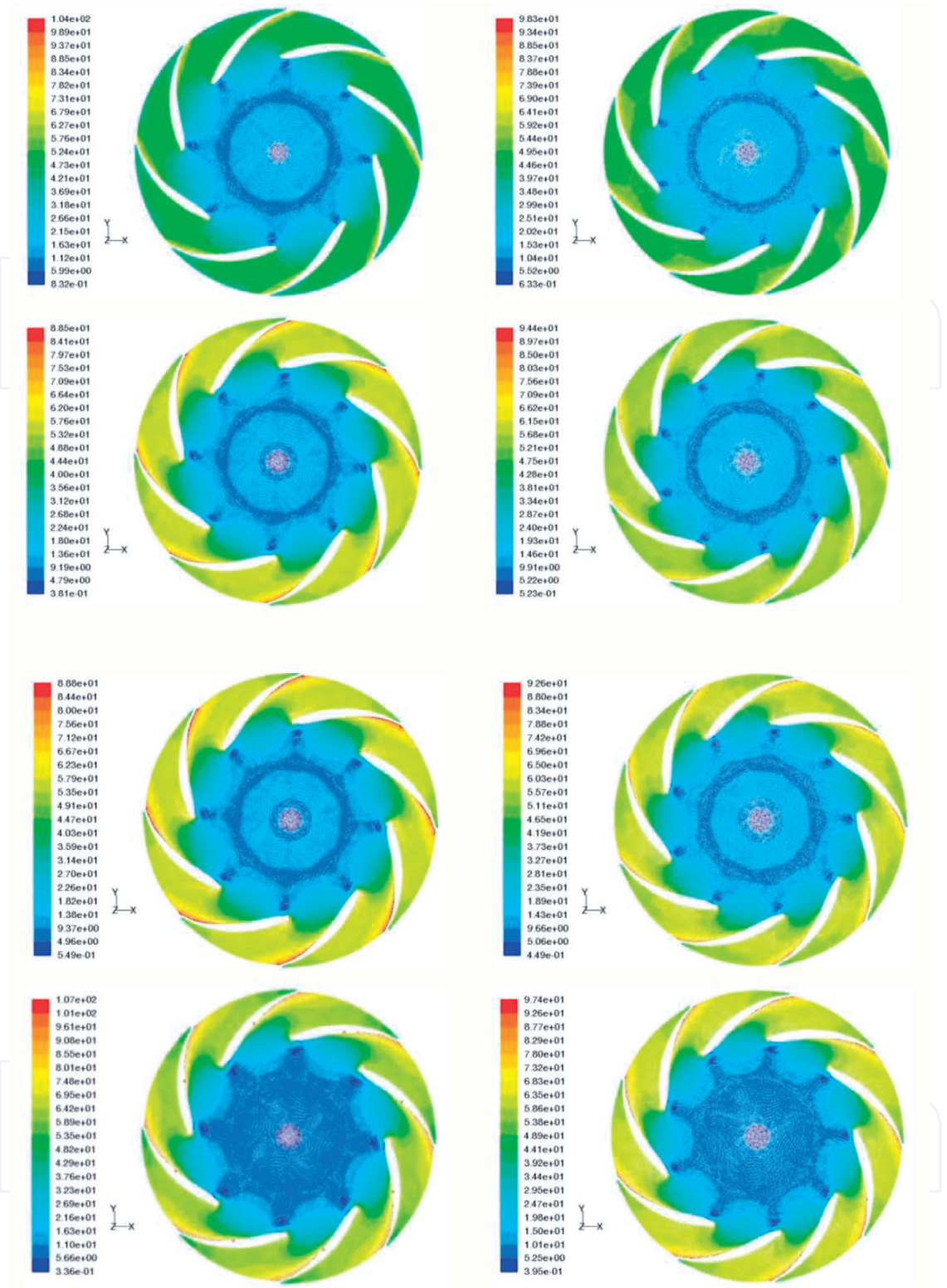


Figure 10.
Total velocity [m/s] distribution for calculated impeller operating points with eight and nine vanes.

For the calculations, the model of impeller according to the enclosed documentation was used as the output model. Calculations have been made for both impeller variants. For both of the cases, the discrete model was based on tetrahedral elements (as exemplary shown in **Figure 8**). Elements near walls were compacted. The flow was modelled as turbulent, using the RANS method and the two-equation turbulence model k-ε.

In the first stage of the study, the analysis of the impeller with eight (**Figure 6**) and nine (**Figure 7**) vanes was carried out. For the eight vanes, the results of the simulation were also compared with the available results in the technical

documentation and found to be similar (**Figure 9**). Furthermore, the overall performance of the two types of impellers found with aid of CFD calculation maintains in similar level.

In order to verify the correctness of the calculation of the main dimensions of the impeller, a theoretical design process was carried out. On the basis of known designs, the influence of impeller parameters on its performance, compression and efficiency was simulated. It was necessary to maintain the existing parameters of the impeller, improving only its efficiency. The modifications were limited by the external dimensions of the impeller in order to be able to work with the existing collecting volute.

After a number of variant combinations, the outlet angle of the vane was changed to 23° and the vane profile modified to improve efficiency. The results show that by changing the outlet angle, the average efficiency for the eight-vane impeller was increased by 2.3% and for the nine-vane impeller by 2.9% in relation to the basic eight-vane impeller.

Figure 10 shows a comparison of the flow images for the impellers with eight and nine vanes with a 23° outlet angle.

The best results were obtained for the nine-vane impeller and the changed outlet angle. An average efficiency increase of 2.9% was achieved in relation to the impeller from the technical documentation. The flow images are correct. There are no particularly dangerous phenomena, such as interruption of flow or turbulence.

4. Centrifugal pump with collecting channel: undetermined flow with cavitation

Another object of the study was a single-stage centrifugal pump with a spiral volute cooperating with two similar types of impellers, commonly used in such a device. Those impellers are denoted as W13 and W17. The W17 impeller differs from the W13 impeller only by the shape of a vane. Both impellers had eight vanes each. The analysis of the impellers with the two-dimensional peculiarity method for non-viscous medium suggested higher cavitation resistance of the W13 impeller.

In the first stage, calculations were made of the undetermined flow through the pump without cavitation in order to determine the most favourable boundary conditions to be applied when analysing the flow through the pump and determining the calculation characteristics of the pump and the impeller.

The calculations reflect the full three-dimensional geometry of the pump (**Figure 11**) consisting of a straight section of the pipeline before the inlet to the impeller, a centrifugal impeller, a spiral collecting volute, a diffuser, and a short section of pipeline after the pump.

Separate discreet models have been built in the inlet and outlet impeller areas. On the cylindrical surface between the impeller and the volute, these models were not connected by common nodes and remained unfit. Thus, during the calculation it was possible to use the "sliding mesh" technique, which is used to model the rotation of the impeller in relation to the stationary casing. The discrete model is built with approximately 1.3 million tetrahedral elements in total. The elements were also compacted near the vane surface and in the area between the impeller and the collecting channel (**Figure 12**).

The mathematical model of the flow is described by the Reynolds-averaged Navier-Stokes equations (RANS). For the description of the turbulence, a two-equation k-ε model was used. The following control surfaces were used, where static pressure was monitored during the calculation:

DOI: http://dx.doi.org/10.5772/intechopen.82266

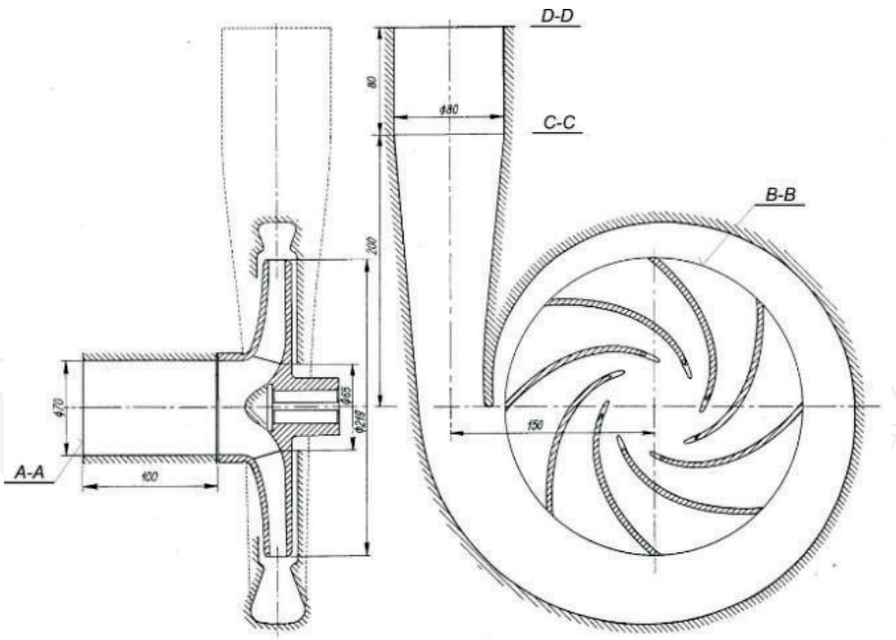


Figure 11.
The calculation area under consideration and its characteristic cross sections (W13 impeller pump).

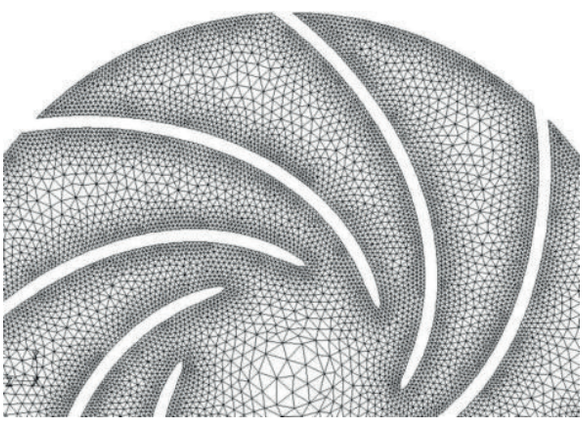


Figure 12.
Discrete model by type of tetrahedral element of the impeller surface, on the hub and rear disc side.

- The inlet section at the beginning of the suction channel (A-A)
- The cylindrical surface at the outlet from the impeller inter-vane channel (B-B)
- The cross section at the end of the diffuser (C-C)
- The outlet section at the end of the cylindrical section of the pipeline (D-D)

Calculations were made according to the scheme:

In the inlet section (A-A), a homogeneous velocity field was set with the value resulting from the flow rate and the channel section area c = Q/A and the direction corresponding to the connector axis ("velocity inlet" boundary condition). In cross section (D-D), a high static pressure of 1000 kPa was set so that the pressure in the impeller would not drop below the saturation vapour pressure ("pressure outlet" boundary condition). A two-phase flow "mixture" model was selected for the calculations. During the calculations, equations describing the formation of the gaseous phase (cavitation) were excluded. This approach is suggested by ANSYS Fluent.

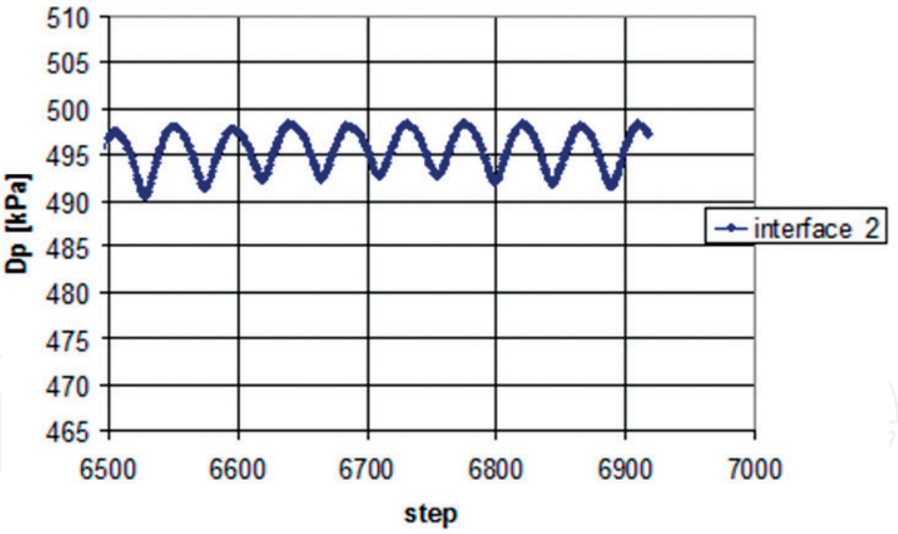


Figure 13.
Example pressure pulsation diagram as pressure difference between vane outlet (interface_2) and inlet (inlet), depending on iteration (time).

On the internal walls of the flow channel, the condition of zero velocity of the fluid in relation to the wall was set. The increase of static pressure (increase of hydrostatic height) between inlet and outlet cross sections of the pump was the expected value and allowed to reproduce flow characteristics. During the calculations, the average static pressure was monitored on the four control surfaces mentioned above. The calculations were interrupted after repeated oscillations of the static pressure on these surfaces were obtained, which took place after 6–8 rotations of the impeller. An example of a pressure pulsation diagram is shown in **Figure 13**. A fixed time step of Δt = 5,75E–5 s, corresponding to an impeller rotation by 1°, was used for the calculations.

The calculated flow characteristics of the entire pump and the W13 impeller are presented in **Figure 14**. The course of the relevant experimental characteristics is also presented.

The pump characteristics indicate a pressure increase between the cross sections A-A and C-C, characteristics of the impeller—between sections A-A and B-B. The pressure drop in the suction channel is insignificant compared to the pressure drop in the impeller.

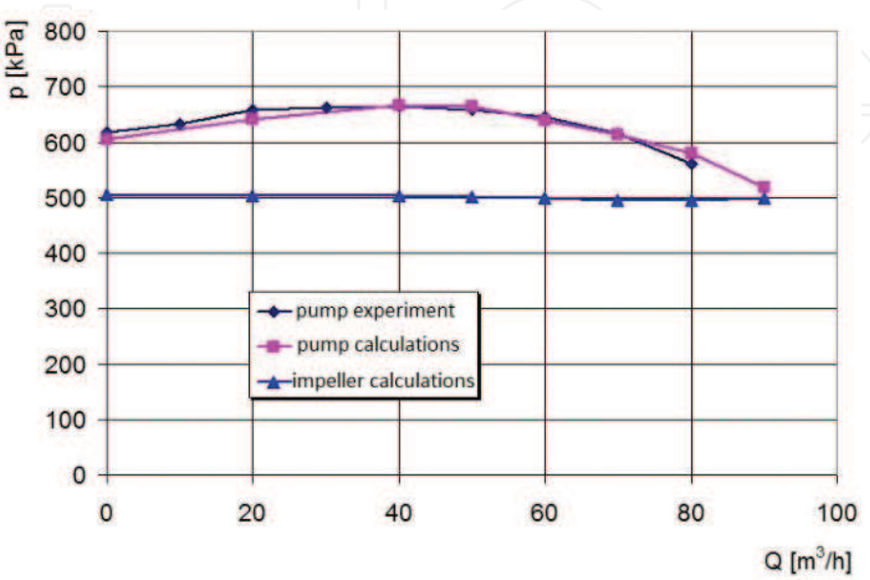


Figure 14.
Pump and impeller flow characteristics W13 determined by calculation of the transient flow (spiral collecting channel model): comparison with experimental data.

Cavitation in the pump is associated with a pressure drop in the suction area of the first degree [11]. This causes the fluid-vapour biphasic flow to occur and the continuity of the flow through the pump to be interrupted. In centrifugal pumps, cavitation shall be characterised by a clearly visible disturbance in the following characteristics: flow H = f(Q), power consumption P = f(Q) and efficiency η = f(Q). If the suction height increases at a given velocity and flow rate (or the intake height decreases), then the boundary value of the suction height at which the pump enters the cavitation state is obtained. In this way, taking into account a certain safety margin, it is possible to obtain a curve of the required excess of the energy of a fluid at the pump inlet section over the energy of evaporation of this fluid in the form of NPSH = f(Q) (net positive suction head). The NPSH parameter expresses the "suction power" of the pump:

$$NPSH = \frac{p_s - p_v}{\gamma} + \frac{c_s^2}{2g} \tag{2}$$

where p_s is the absolute pressure at the inlet cross section of the pump and c_s is the fluid velocity at the pump inlet cross section (average). Typically, this surplus is related to a state where the first-stage total head drops by 3% (NPSH3).

Determination of the cavitation state in the impeller for a given flow rate requires many calculations of the pressure distribution in the inter-vane space at the decreasing inlet pressure. The simulation assumes that a simplified geometric model of a collective channel can be used to determine the flow characteristics of the impeller itself. Instead of a spiral, an axial-symmetrical guide was used as a drainage element for the medium.

Due to the symmetry of geometry, the flow through the impeller is determined. The elimination of pressure pulsations has significantly accelerated the iterative calculation process. The flow field in the impeller still remained a periodic-symmetric field, but it was the same in all the vane channels. This allowed the calculation area to be limited to one inter-vane channel of the impeller. As a result, the calculation time corresponding to one characteristic point has been reduced.

A discrete model consisting of about 300,000 hexahedral cells was used. Since the discrete model remains stationary during the calculation, a *moving reference frame* was used which rotates at the impeller velocity.

For the calculations, the "velocity inlet" and "pressure outlet" boundary conditions were used on the outer surface of the annular collecting channel and the two-phase flow "mixture" model. During the calculation, the average static pressure value at the cross sections A-A (inlet) and B-B (outlet from the impeller inter-vane channel) was monitored.

Cavitation test in the impeller was performed for several selected values of the flow rate. Calculations were carried out in which equations describing cavitation and two-phase flow were included. The static pressure at the outlet was gradually reduced from 800 to 580 kPa.

It was found that the lowest pressure in the impeller was initially higher than the saturated vapour pressure $p_{min} > p_v$; then it was already limited by the p_v value. For each set outlet pressure, the static inlet pressure was recorded. In the W13 impeller, cavitation occurs on the impeller vanes, close to the incidence edge on the concave side of the vane. In the W17 impeller, cavitation appears on the convex side of the vane (for Q = 70 m^3/h). Selected images of the development of cavitation are presented in **Figures 15** and **16**.

When the outlet pressure is further reduced, it reaches a constant boundary value, depending on the flow rate—fully developed cavitation. Further lowering of the outlet pressure leads to a loss of convergence and interruption of the calculation.

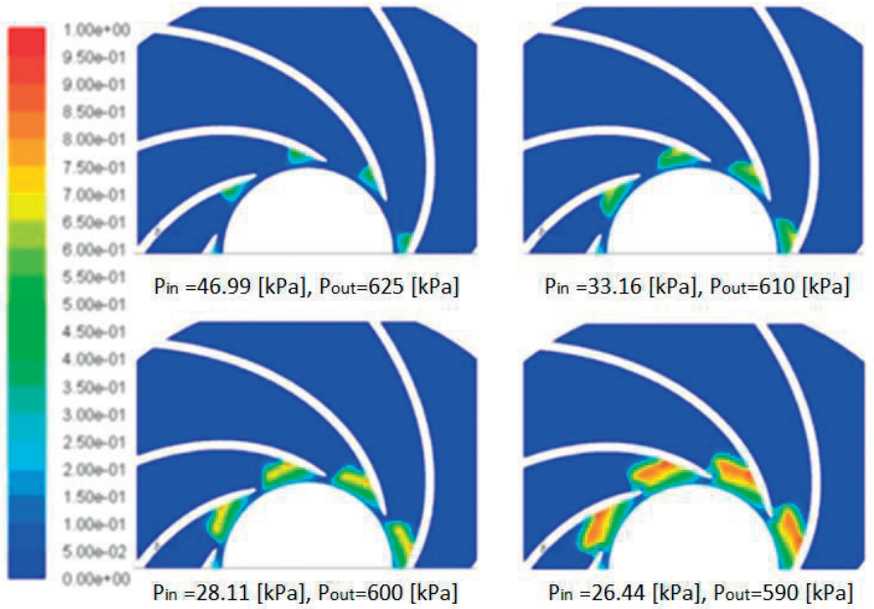


Figure 15.
Cavitation development image on the impeller W13 disc surface at Q = 70 m³/h and decreasing static pressure at the inlet (percentage of gas phase is given).

Cavitation image – model with spiral collection channel and immovable impeller (*Moving Reference Frame*) – **Figure 17**. Cavitation image – model with spiral collecting channel and rotating impeller (*Moving Mesh*) – **Figure 18**.

The cavitation fields for the axial-symmetric model are correctly symmetrical. However, the behaviour of the tested impellers is different:

- Impeller W13: cavitation is formed on the concave side of the vane.
- Impeller W17: cavitation is formed on the convex side of the vane.

The calculations converge quickly. However, the cavitation fields in the *moving reference frame* model are non-physical, and the cavitation area expands very

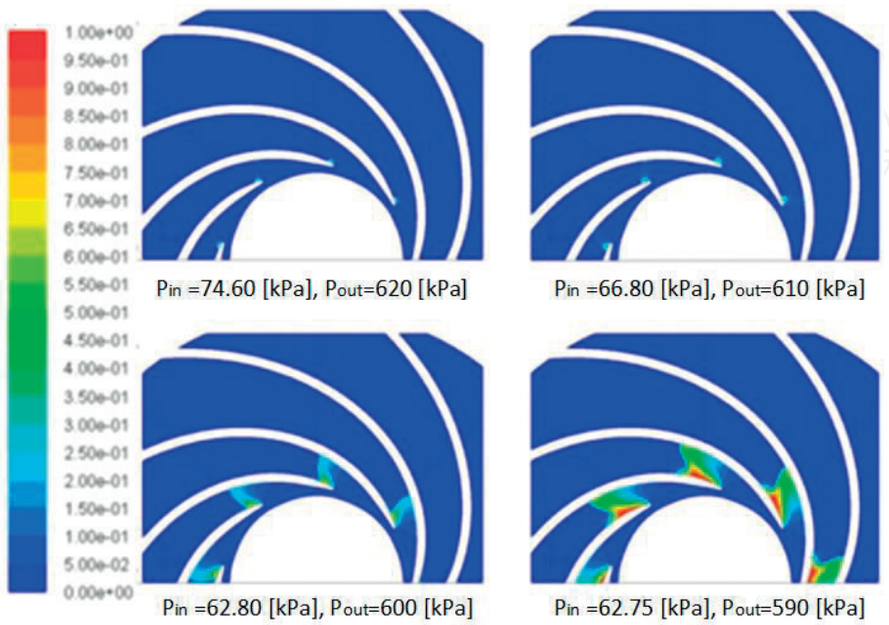


Figure 16.
Cavitation development image on the impeller W17 disc surface at Q = 70 m³/h and decreasing static inlet pressure (percentage of gas phase is given).

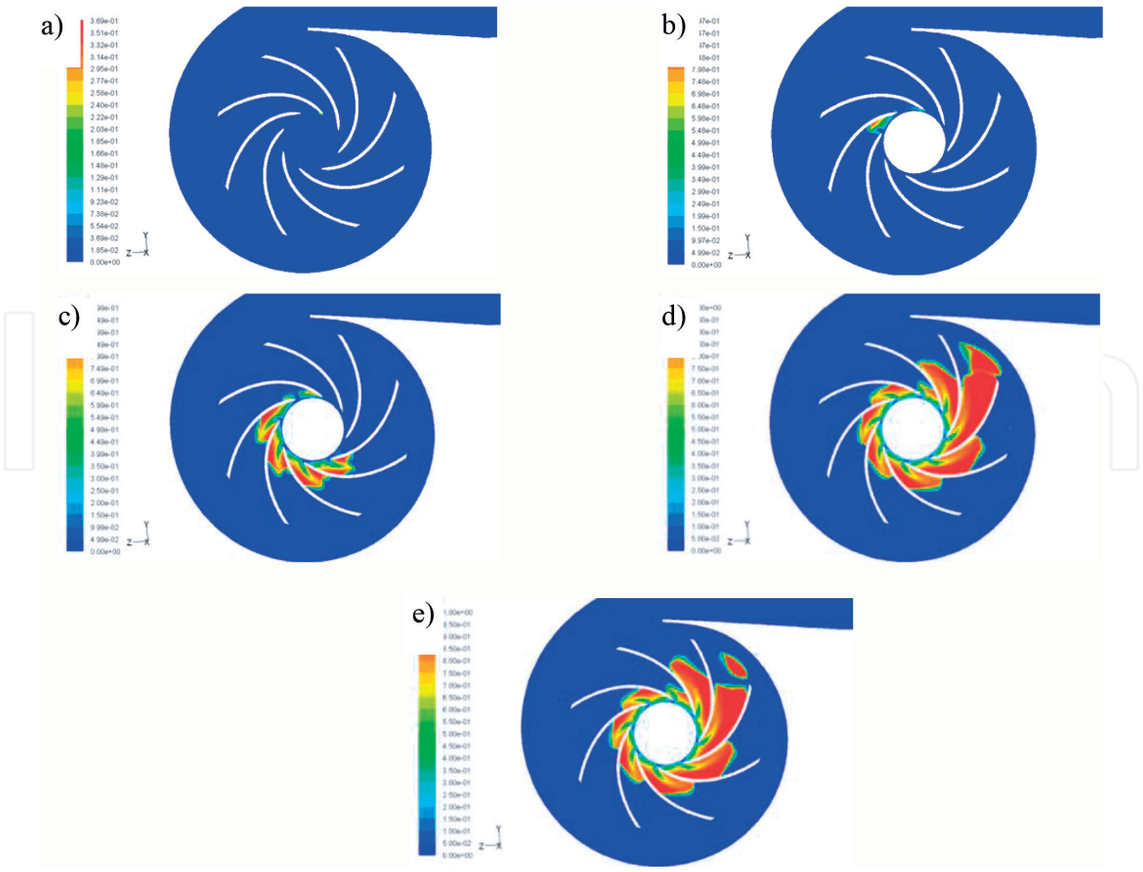


Figure 17.
Cavitation area for parameters: (a) inlet = 189 kPa and outlet = 800 kPa, (b) inlet = 95 kPa and outlet = 700 kPa, (c) inlet = 58 kPa and outlet = 650 kPa, (d) inlet = 27 kPa and outlet = 622 kPa and (e) inlet = 27 kPa and outlet = 600 kPa. The percentage of gas phase is given.

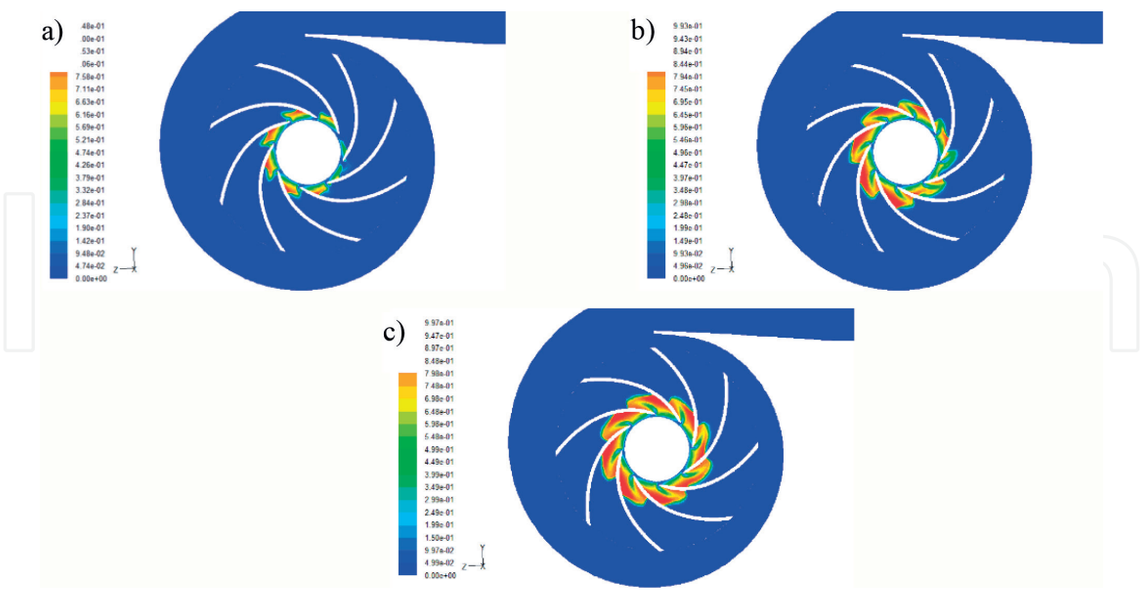


Figure 18.
Cavitation area for parameters: (a) inlet = 28.3 kPa and outlet = 675 kPa, (b) inlet = 27.8 kPa and outlet = 650 kPa and (c) inlet = 27.8 kPa and outlet = 622 kPa. The percentage of gas phase is given.

quickly. Cavitation starts in the direction of the smallest radius of the collecting spiral. The *moving mesh* model produces the best results (mainly physical). However, the problem is the slow convergence of calculations and their long duration.

5. Cavitation resistance of the pump

The different cavitation properties of the two impellers can be explained by the significantly different inlet angle of the β1 vane—30°40′ (W13) and 21° (W17)—as with the same other geometric data, resulted in a very different position of the ideal inflow point. This is confirmed by the experimental characteristics of the pumps $H = f(Q)$ and $\eta = f(Q)$ from operation.

The analyses indicated the possibility of obtaining information on cavitation resistance of the designed structure through the rational use of CFD programs. The alternative solution of designing a prototype pump and carrying out a series of experiments may be challenging.

6. Conclusion

The CFD analysis made it possible to identify areas where cavitation is more likely to occur and to assess its intensity in relation to the rotational velocity. The results showed that one of the inlet channels has both negative pressure and increased fluid flow velocity. Calculations made for different pump rotational velocities and different suction channel geometries have shown that the intensity of these phenomena increases with the rotational velocity. However, these phenomena are not strong enough to contribute to the development of the phenomenon of cavitation. A series of simulations for different suction channel geometries have confirmed that no modification of the suction channel geometry is required. Considering the designs presented here the cavitation occurred either on the convex or concave side of the vane. The main difference between the vanes was the angle of its inclination. Hence there is a specific angle between 30 and 21° at which the transition occurs. The volumetric flow rate was unchanged in both of the impeller designs, although the inlet pressures were found to be different. For blades inclined at 30°, the inlet pressures were almost twice lower than in the case of 21°. Hence lower inclination of blades is more immune to cavitation development.

The CFD calculations were made to check the selection of the main dimensions of the radial fan. After performing many variant calculations, it was found that by changing the number of blades and the outlet angle of the blades, it is possible to increase the efficiency of the fan. It appeared that the efficiency is greater for impellers with greater amount of vanes. Furthermore the efficiency increased when the vanes were inclined to 23°, and as stated above, at such angle the cavitation occurs at higher inlet pressures and represent higher immunity to cavitation. Therefore the increase of efficiency may be partially a consequence of lack of cavitation.

It was found that the characteristics of the centrifugal pump from CFD calculations are consistent with the characteristics obtained experimentally. Based on the CFD analysis, cavitation resistance of the designed centrifugal pump was determined.

DOI: http://dx.doi.org/10.5772/intechopen.82266

IntechOpen

IntechOpen

Author details

Wieslaw Fiebig*, Paulina Szwemin and Maciej Zawislak
Faculty of Mechanical Engineering, Wroclaw University of Science and Technology, Wroclaw, Poland

*Address all correspondence to: wieslaw.fiebig@pwr.edu.pl

IntechOpen

© 2018 The Author(s). Licensee IntechOpen. This chapter is distributed under the terms of the Creative Commons Attribution License (http://creativecommons.org/licenses/by/3.0), which permits unrestricted use, distribution, and reproduction in any medium, provided the original work is properly cited. CC BY

References

[1] Fiebig W, Cependa P, Jedraszczyk P, Kuczwara H. Innovative solution of an integrated motor pump assembly. In: ASME/BATH 2017 Symposium on Fluid Power and Motion Control. Sarasota, USA: ASME; 2017

[2] Frosina E. A three dimensional cfd modeling methodology applied to improve hydraulic components performance. Energy Procedia. 2015;**82**:950-956

[3] Mancò S, Nervegna N, Rundo M, Armenio G. Modelling and Simulation of Variable Displacement Vane Pumps for IC Engine Lubrication, SAE Technical Paper 2004-01-16012004

[4] Inaguma Y. Theoretical analysis of mechanical efficiency in vane pump. JTEKT Engineering Journal, English Edition No. 1007E Technical paper. 2010:28-35

[5] Frosina E, Stelson KA, et al. Vane pump power split transmission: Three dimensional computational fluid dynamics modeling. In: ASME/BATH 2015 Symposium on Fluid Power & Motion Control. Chicago, USA; 2015

[6] Houzeaux G, Codina R. A finite element method for the solution of rotary pumps. Computers and Fluids. 2007;**36**:667-679

[7] Hyun K, Hazel M, Suresh P. Two-Dimensional CFD Analysis of a Hydraulic Gear Pump. Washington: American Society for Engineeguide Education; 2007

[8] Mochala M. Intermittent CFD simulation of interlocked hydraulic pumps industrial use, basic conditions and prospect. In: FLUIDON Konferenz "Simulation in mechanischen Umfeld", Aachen; 2009

[9] Stryczek J et al. Visualisation research of the flow processes in the outlet chamber—outlet bridge—inlet chamber zone of the gear pumps. Archives of Civil and Mechanical Engineering. 2014;**15**(1):95-108. DOI: 10.1016/j.ACME 2014.02.010

[10] Jedraszczyk P, Fiebig W. CFD Model of an External Gear Pump Proceedings of 13th International Conference Computer Aided. Springer International Publishing; 2017. Available from: https://www.spguideerprofessional.de/en/cfd-model-of-an-external-gear-pump/12181546

[11] Tabaczek T, Zawiślak M, Zieliński AK. Flow and cavitation analysis of a centrifugal pump. Systems: Journal of Transdisciplinary Systems Science. 2012;**16**(2):385-394